

Supporting Information

Facilitating Intrinsic Delayed Fluorescence of Conjugated Emitters by Inter-Chromophore Interaction

Yixuan Gao,^{a,†} Yingman Sun,^{b,†} Zilong Guo,^a Guo Yu,^a Yaxin Wang,^a Yan Wan,^c Yandong Han,^d Wensheng Yang,^d Dongbing Zhao^{b,*} and Xiaonan Ma^{a,*}

^a Institute of Molecular Plus, Tianjin University, Tianjin 300072, P. R. China;

^b State Key Laboratory and Institute of Elemento-Organic Chemistry, College of Chemistry, Nankai University, Tianjin 300071, P. R. China;

^c College of Chemistry, Beijing Normal University, Beijing 100875, P. R. China;

^d Engineering Research Center for Nanomaterials, Henan University, Kaifeng 475004, P. R. China.

[†]These authors contributed equally.

*dongbing.chem@nankai.edu.cn

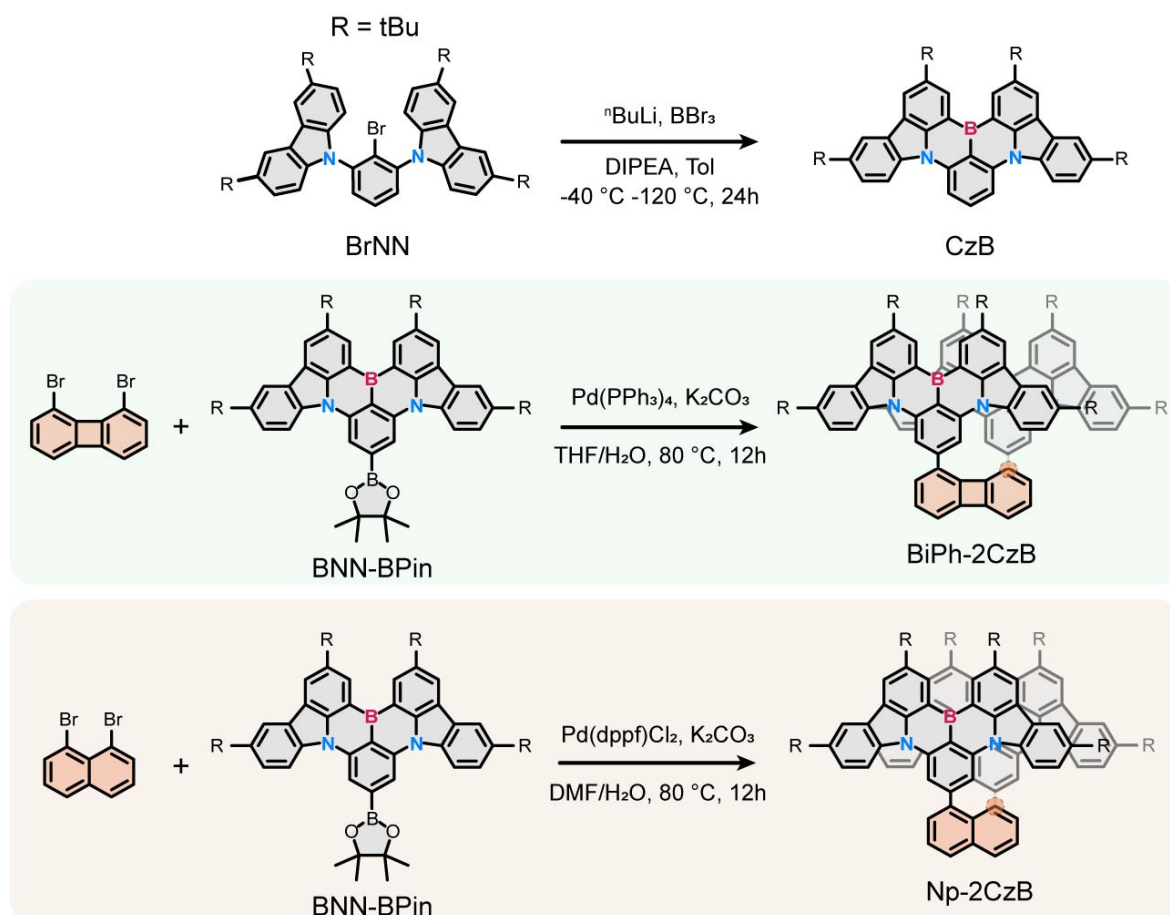
*xiaonanma@tju.edu.cn

Contents

| Section | Content | Page |
|---------|-------------------------------------------------------------|------|
| S1 | Synthesis | 3 |
| | Scheme S1 | 3 |
| | Fig. S1 | 5 |
| | Fig. S2 | 5 |
| | Fig. S3 | 6 |
| | Fig. S4 | 6 |
| S2 | Characterization and calculation | 7 |
| S3 | Optimal geometrical structure | 10 |
| | Table S1 | 10 |
| S4 | Steady spectra | 11 |
| | Fig. S5 | 11 |
| | Fig. S6 | 12 |
| S5 | Time-resolved Fluorescence | 13 |
| | Fig. S7 | 13 |
| S6 | Reported k_{RISC} values of reported TADF emitters | 14 |
| | Table S2 | 14 |
| | Table S3 | 15 |
| S7 | Calculated and experimentally measured excitation energy | 16 |
| | Fig. S8 | 16 |
| S8 | Reduced density gradient (RDG) analysis | 17 |
| | Fig. S9 | 17 |
| S9 | Vibrational analysis | 18 |
| | Fig. S10 | 18 |
| | Fig. S11 | 18 |
| S10 | Excitation-dependent fluorescence spectra | 19 |
| | Fig. S12 | 19 |
| | Fig. S13 | 20 |
| S11 | fs-TA spectra | 21 |
| | Fig. S14 | 21 |
| | Fig. S15 | 22 |
| | Fig. S16 | 23 |
| | Fig. S17 | 24 |
| | Fig. S18 | 25 |

Section S1. Synthesis

All chemicals and materials, unless otherwise noted, were commercially available and used without further purification. 1,8-Dibromobiphenylene and BNN-BPin were prepared by following literature methods.^{1,2}



Scheme S1. The synthetic route of CzB, BiPh-2CzB and Np-2CzB.

CzB: In a 250 mL Schlenk flask, **BrNN** (7.10 g, 10 mmol) and 80 mL dry toluene were added under nitrogen. $n\text{BuLi}$ (4.8 mL, 12 mmol, 2.5 M in hexane) was dropwise added at 0 °C. After stirring at room temperature for 1 hour, the mixture was cooled down to -40 °C again, and BBr_3 (1.5 mL, 15 mmol) was slowly added. After the mixture was stirred at room temperature for 2 hour, *N,N*-Diisopropylethylamine (3.6 mL, 20 mmol) was added at 0 °C. The mixture was heated to 120 °C and stirred for 24 hours. Cooled down the mixture to room temperature, carefully quenched by addition of water, and extracted by CH_2Cl_2 three times. The organic layer was dried by Na_2SO_4 , concentrated in vacuum, and purified by flash chromatography on silica gel with petroleum ether/ CH_2Cl_2 (10:1, v/v) and recrystallization from DCM/MeOH to give **CzB** as a yellow solid, 2.32 g, 36.2% yield.

^1H NMR (400 MHz, CDCl_3) δ 9.13 (d, J = 1.8 Hz, 2H), 8.47 (d, J = 1.8 Hz, 2H), 8.39 (d, J = 8.8 Hz, 2H), 8.32 (d, J = 8.4 Hz, 2H), 8.27 (d, J = 1.9 Hz, 2H), 8.00 (t, J = 8.3 Hz, 1H), 7.65 (dd, J = 8.8, 2.0 Hz, 2H), 1.67 (s, 18H), 1.54 (s, 18H). **^{13}C NMR (101 MHz, CDCl_3)**

δ 145.26, 144.60, 144.27, 141.53, 138.35, 133.01, 129.80, 127.04, 124.33, 123.61, 120.64, 117.24, 114.08, 107.93, 35.16, 34.78, 32.19, 31.82.

BiPh-2CzB: In a 25 mL Schlenk flask, 1,8-dibromobiphenylene (34.0 mg, 0.11 mmol), **BNN-BPin** (0.19 g, 0.24 mmol), Pd(PPh₃)₄ (12.7 mg, 0.011 mmol) and K₂CO₃ (60.8 mg, 0.44 mmol) were added under nitrogen. After adding 5.0 mL THF and 0.9 mL H₂O under nitrogen, the mixture was heated to 80 °C and stirred for 12 hours. The reaction mixture was cooled to room temperature and extracted by CH₂Cl₂ three times. The organic phase was dried over Na₂SO₄ and the solvent was evaporated in vacuo. The crude product was purified by flash chromatography on silica gel with petroleum ether/CH₂Cl₂ (5:1, v/v) and recrystallization from DCM/MeOH to give **BiPh-2CzB** as a yellow solid, 21.2 mg, 13.5% yield.

¹H NMR (400 MHz, CDCl₃) δ 8.46 (d, *J* = 1.8 Hz, 4H), 8.03 (d, *J* = 1.7 Hz, 4H), 7.88 (s, 4H), 7.72 (d, *J* = 8.8 Hz, 4H), 7.62 (d, *J* = 2.0 Hz, 4H), 7.25 (d, *J* = 2.0 Hz, 2H), 7.22 (d, *J* = 2.0 Hz, 2H), 7.21 (s, 1H), 7.19 (s, 1H), 7.12 (d, *J* = 6.8 Hz, 1H), 7.10 (d, *J* = 6.8 Hz, 1H), 6.94 (s, 1H), 6.93 (s, 1H), 1.63 (s, 36H), 1.22 (s, 36H).

¹³C NMR (101 MHz, CDCl₃) δ 151.52, 148.57, 144.36, 143.39, 143.36, 141.93, 141.01, 137.58, 134.47, 130.68, 129.43, 129.18, 126.78, 123.37, 123.04, 121.08, 119.87, 116.34, 116.26, 113.85, 108.71, 35.00, 34.35, 32.39, 31.51.

HRMS (MALDI) calcd for C₁₀₄H₁₀₂B₂N₄ [M+H]⁺: 1429.8369, Found: 1429.8388.

Np-2CzB: In a 25 mL Schlenk flask, 1,8-dibromonaphthalene (28.6 mg, 0.1 mmol), **BNN-BPin** (0.17 g, 0.22 mmol), Pd(dppf)Cl₂ (7.2 mg, 0.01 mmol), K₂CO₃ (55.3 mg, 0.4 mmol) were added under nitrogen. After adding 4.0 mL DMF and 1.0 mL H₂O under nitrogen, the mixture was heated to 80 °C and stirred for 12 hours. The reaction mixture was cooled to room temperature and extracted by CH₂Cl₂ three times. The organic phase was dried over Na₂SO₄ and the solvent was evaporated in vacuo. The crude product was purified by flash chromatography on silica gel with petroleum ether/CH₂Cl₂ (5:1, v/v) and recrystallization from DCM/MeOH to give **Np-2CzB** as a yellow solid, 51.2 mg, 36.4% yield.

¹H NMR (400 MHz, CDCl₃) δ 8.28 (d, *J* = 1.7 Hz, 4H), 8.22 (d, *J* = 1.2 Hz, 1H), 8.20 (d, *J* = 1.3 Hz, 1H), 7.98 (d, *J* = 1.6 Hz, 4H), 7.95 (s, 4H), 7.76 – 7.70 (m, 10H), 7.66 (d, *J* = 1.1 Hz, 1H), 7.64 (d, *J* = 1.2 Hz, 1H), 6.91 (dd, *J* = 8.7, 2.0 Hz, 4H), 1.63 (s, 36H), 1.39 (s, 36H).

¹³C NMR (101 MHz, CDCl₃) δ 147.44, 143.59, 143.09, 142.33, 141.39, 140.79, 137.56, 134.85, 130.53, 129.43, 129.01, 128.91, 126.35, 125.19, 123.26, 122.76, 121.37, 121.06, 119.64, 116.60, 113.31, 110.24, 34.91, 34.41, 32.34, 31.73.

HRMS (MALDI) calcd for C₁₀₂H₁₀₂B₂N₄ [M]⁺: 1404.8285, Found: 1404.8281.

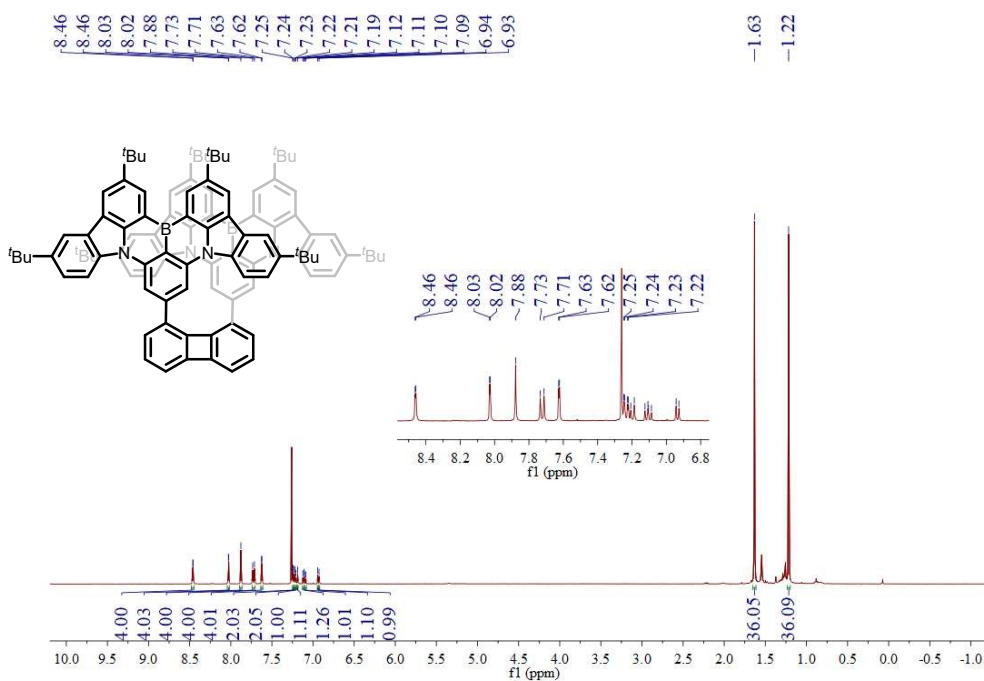


Fig. S1 ¹H NMR spectrum of **BiPh-2CzB** (400 MHz, CDCl₃).

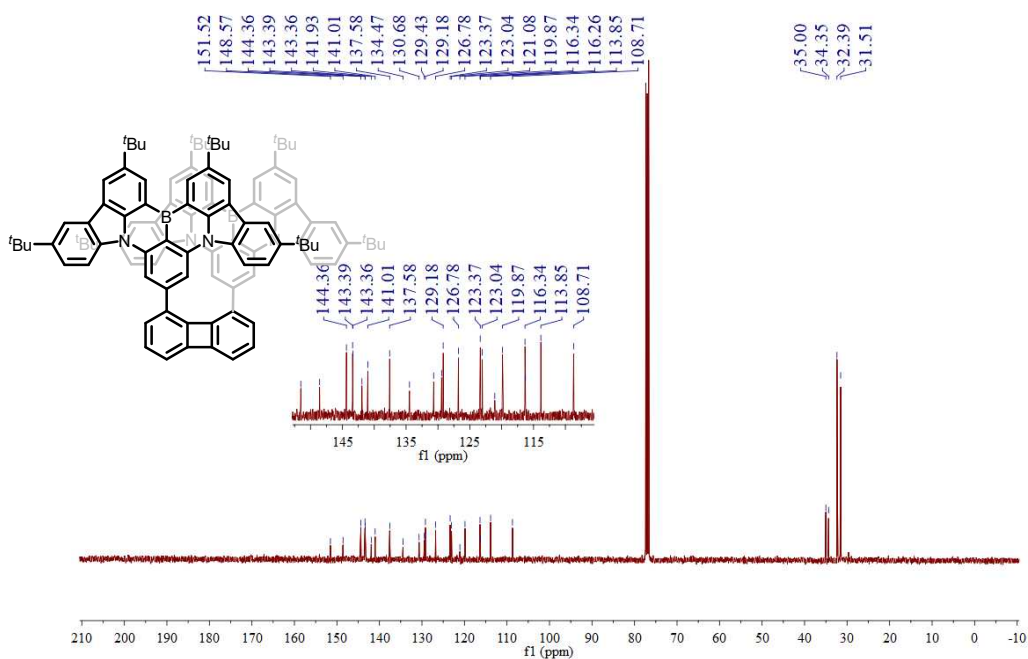


Fig. S2 ¹³C NMR spectrum of **BiPh-2CzB** (101 MHz, CDCl₃).

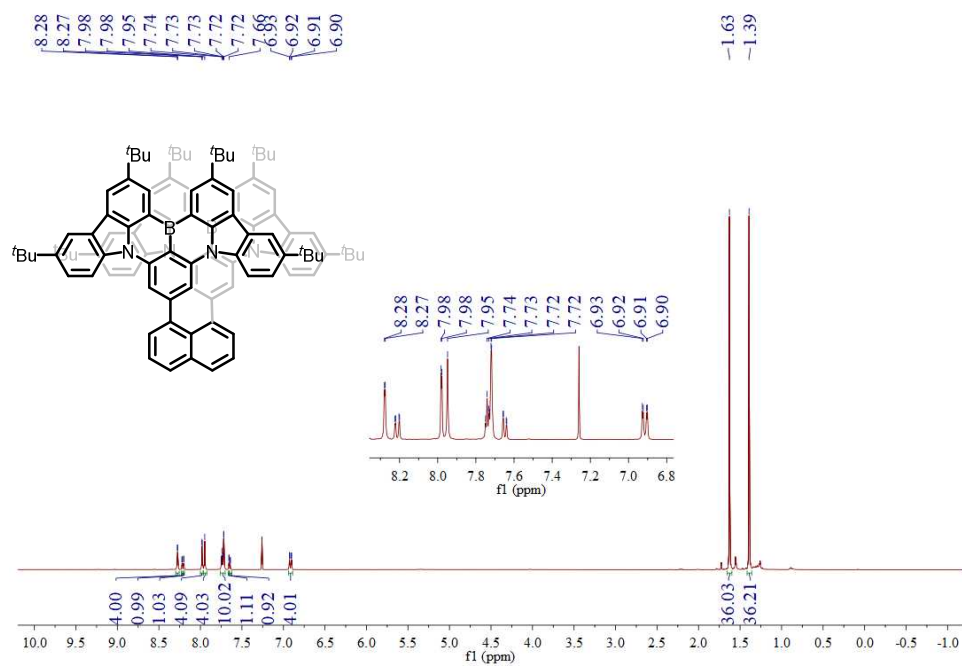


Fig. S3 ¹H NMR spectrum of **Np-2CzB** (400 MHz, CDCl₃).

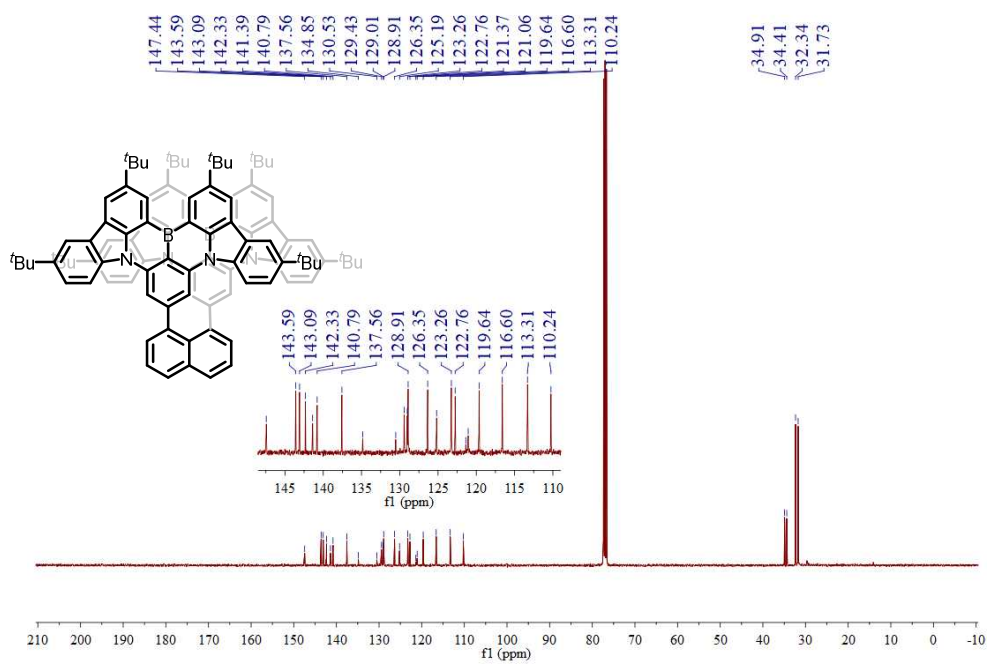


Fig. S4 ¹³C NMR spectrum of **Np-2CzB** (101 MHz, CDCl₃).

Section S2. Characterization and calculation

Chemical and materials. All involved organic solvents are HPLC grade and used as received. For fabricating PMMA doping films of CzB, BiPh-2CzB and Np-2CzB, PMMA solutions were firstly prepared by dissolving 1 g PMMA in 11.5 mL toluene. The resulted PMMA solution (2 mL) was then mixed with 3 mg materials, corresponding to 2wt% doping concentration. The two-step dissolving was performed with stirring (400 rpm) at room temperature. The PMMA solution of CzB, BiPh-2CzB and Np-2CzB were further spin-coated (1000 rpm, 1 min) on 1 mm thick quartz substrates with 1000 rpm/s acceleration, resulting in doping films with absorbance of 0.2–0.3 at excitation wavelength of CzB, BiPh-2CzB and Np-2CzB.

Steady and time-resolved fluorescence spectra. The steady-state UV/Vis absorption and photoluminescence spectra were recorded on U-3900 (Hitachi, Japan) spectrophotometer and F-4700 (Hitachi, Japan) fluorescence spectrometer, respectively. The fluorescence quantum yield (Φ_F) of solution was determined by using 9,10-Bis(phenylethynyl)-anthracene (BPEA, $\Phi_F = 1.0$, in toluene) as a reference.³ For oxygen-free measurements, solutions were bubbled with nitrogen flow for 15 min before measurements. The Φ_F of PMMA doping films were measurements by an integrating sphere with CW excitation at 365 nm. The prompt fluorescence time traces of solution and doping films were recorded with a time correlated single-photon counting (TCSPC) spectrometer (PTI Quanta Master 800, HORIBA) equipped with a 330 nm nano-LED excitation source, which leads to an instrument response function (IRF) value of 0.6 ns. The delayed fluorescence time traces were measured by SpectraLED equipped with a 355 nm excitation source. The phosphorescence spectra were measured by the Edinburgh Instruments FLS1000 with 77 K, and the PF and DF components were screened by time-gating of 50 ms delay.

Estimating of decay rates of S_1 and T_1 states. In our study, the ISC rate constant (k_{ISC}) are all significantly larger than both the rate constants of nonradiative decay from a triplet excited state (k_{nr}^T) and k_{RISC} . According to the fluorescence decay traces, the radiative decay from triplet excited states (k_r^T) does not occur at room temperature in our system. Thus, we assumptions that $k_r^T = k_{nr}^T = 0$, then the decay rates (k_r^S , k_{nr}^S , k_{ISC} and k_{RISC}) of CzB, Biph-2CzB and Np-2CzB emitters were estimated by method introduced by Adachi et al.,^{4,5} the involved formulas are:

$$k_r^S = \frac{\Phi_{PF}}{\tau_{PF}} \quad (1)$$

$$k_{PF} = \frac{1}{\tau_{PF}} \quad (2)$$

$$k_{ISC} = k_{PF} \cdot \Phi_{ISC} = k_{PF} \cdot \frac{\Phi_{DF}}{\Phi_F} \quad (3)$$

$$k_{nr}^S = k_{PF} - k_r^S - k_{ISC} \quad (4)$$

$$k_{RISC} = \frac{(k_{PF} + k_{DF})}{2} - \sqrt{\frac{(k_{PF} + k_{DF})^2}{2} - k_{PF} \cdot k_{DF} \cdot \left(1 + \frac{\Phi_{DF}}{\Phi_{PF}}\right)} \quad (5)$$

fs-TA spectra. The fs-TA measurements were performed by using home-built ultrafast pump-probe spectrometer upon 320 nm optical excitation. Briefly, a commercial 1 kHz Ti:sapphire laser system delivered ~40 fs pulses centered at 800 nm. The ~60 fs excitation pulses ($\lambda_{\text{pump}} = 320$ nm) were derived from the second-harmonic output of a collinear optical parametric amplifier. Approximately 0.1–0.2 μJ pulse energy was measured at the sample position. The broadband UV/Vis probe pulses were generated by focusing a small portion of the Ti:sapphire laser fundamental into a linearly moving CaF_2 window, resulting in a white-light spectrum between 350 nm and 750 nm. Pump and probe beams were spatially overlapped in a quartz cuvette with 500 μm sample thickness or in PMMA films directly, optical density of sample was controlled to 0.1–0.3 at 320 nm. The polarization of pump and probe beams were set to magic angle of 54.7° . After passing the sample, the probe pulses were dispersed in a grating spectrometer and detected by a linear Si detector array. The measured TA data were evaluated via target analysis with software package Glotaran⁶ based on the R-package TIMP.⁷

Electronic structure and wave-function analysis. All electronic structure calculation of CzB, BiPh-2CzB and Np-2CzB were performed using Gaussian 09⁸ and 16⁹ software packages. The geometric structure of investigated emitters was optimized on both ground (S_0), singlet (S_1) excited states at B3LYP/6-31G* level while no imaginary frequency was found by frequency analysis. The vertical (ΔE_{ST}) energy gaps between singlet (S_1) and triplet (T_1) excited states were estimated by single point and geometric optimization calculation, respectively.

Vibrational analysis. The Huang-Rhys (HR) factor (S_k) and reorganization energy contribution (λ_k) of each vibrational modes were calculated by using MOMAP software on basis of frequency analysis of corresponding states.¹⁰ We further estimated reorganization energy contribution (λ_k) of each vibrational modes between S_1 and S_0 states with the harmonic oscillator approximation:

$$\lambda_k = \sum_k \frac{1}{2} \omega_k^2 \Delta Q_k^2 \quad (6)$$

in which λ_k can be calculated by the corresponding frequency (ω_k) and vibrational displacement (ΔQ_k), while ΔQ_k can be estimated as a linear combination of internal coordinates, *i.e.*

$$\Delta Q_k = \sum_j \zeta_{kj} \Delta D_j \quad (7)$$

where ΔD_j represents displacement along the internal coordinate j of the equilibrium position in the $S_1 \rightarrow S_0$ transition. The HR factor (S_k) of each vibrational mode k can be calculated with its frequency (ω_k) and displacement (ΔQ_k).

$$S_k = \frac{1}{2\hbar} \omega_k \Delta Q_k^2 \quad (8)$$

Spin-orbital coupling. The SOC matrix elements between singlet (S_1) and triplet (T_1) excited states were calculated by using the linear-response LR methods implemented in PySOC program,¹¹ which has been included in MOMAP software. The SOC Hamiltonian can be approximately calculated as

$$\hat{H}_{SO} \approx \sum_i^{N_e} \zeta(r_i) \hat{\mu}_L \hat{\mu}_S \quad (9)$$

where $\hat{\mu}_L$ and $\hat{\mu}_S$ represent magnetic moment operators resulting from orbital and spin angular momentum with SOC constant $\zeta(r_i)$.

Reduced density gradient (RDG) analysis. The noncovalent interactions were analyzed through RDG by using Multiwfn program.¹² The corresponding RDG iso-surface were rendered by using the VMD 1.9.3 program.¹³ The RDG distribution is divided into three colors including blue, green and red, which represents strong interactions, van der Waals interactions and repulsion interactions, respectively. Besides, the peaks in the region of $\text{Sign}(\lambda_2)\rho < 0$, $= 0$ and > 0 of the scatter graphs are in the blue, green, and red, respectively.

Reference

- 1 S. M. Kilyanek, X. Fang and R. F. Jordan, *Organometallics*, 2009, **28**, 300–305.
- 2 Y. Xu, C. Li, Z. Li, J. Wang, J. Xue, Q. Wang, X. Cai and Y. Wang, *CCS Chem.*, 2022, **4**, 2065–2079.
- 3 A. Demeter, *J. Phys. Chem. A*, 2014, **118**, 9985–9993.
- 4 Y. Wada, H. Nakagawa, S. Matsumoto, Y. Wakisaka and H. Kaji, *Nat. Photon.*, 2020, **14**, 643–649.
- 5 Y. Tsuchiya, S. Diesing, F. Bencheikh, Y. Wada, P. L. Dos Santos, H. Kaji, E. Zysman-Colman, I. D. W. Samuel and C. Adachi, *J. Phys. Chem. A*, 2021, **125**, 8074–8089.
- 6 I. H. M. Van Stokkum, D. S. Larsen and R. Van Grondelle, *BBA Bioenerg.*, 2004, **1657**, 82–104.
- 7 K. M. Mullen and I. H. M. V. Stokkum, *J. Stat. Soft.*, 2007, **18**, 1-46.
- 8 Frisch, M. J.; Trucks, G. W.; Schlegel, H. B.; Scuseria, G. E.; Robb, M. A.; Cheeseman, J. R.; and Scalmani, G.; Barone, V.; Petersson, G. A.; Nakatsuji, H.; et al., Gaussian 09, Revision D.01 (version Gaussian 09, Revision D.01) Gaussian, Inc., Wallingford CT 2013.
- 9 Frisch, M. J.; Trucks, G. W.; Schlegel, H. B.; Scuseria, G. E.; Robb, M. A.; Cheeseman, J. R.; and Scalmani, G.; Barone, V.; Petersson, G. A.; Nakatsuji, H.; et al., Gaussian 16, Revision A.03 (version Gaussian 16, Revision A.03) Gaussian, Inc., Wallingford CT 2016.
- 10 Y. Niu, W. Li, Q. Peng, H. Geng, Y. Yi, L. Wang, G. Nan, D. Wang and Z. Shuai, *Mol. Phys.*, 2018, **116**, 1078–1090.
- 11 X. Gao, S. Bai, D. Fazzi, T. Niehaus, M. Barbatti and W. Thiel, *J. Chem. Theory Comput.*, 2017, **13**, 515–524.
- 12 T. Lu and F. Chen, *J. Comput. Chem.*, 2012, **33**, 580–592.
- 13 W. Humphrey, A. Dalke and K. Schulten, *J. Mol. Graph.*, 1996, **14**, 33–38.

Section S3. Optimal geometrical structure

Table S1. The DFT and TDDFT (B3LYP, 6-31g*, PCM = toluene) calculated optimal geometrical structures of CzB, BiPh-2CzB and Np-2CzB in both ground and excited-states.

| | | Side view | Front/Top view |
|-----------|----------------|-----------|----------------|
| CzB | S ₀ | | |
| | S ₁ | | |
| BiPh-2CzB | S ₀ | | |
| | S ₁ | | |
| Np-2CzB | S ₀ | | |
| | S ₁ | | |

Section S4. Steady spectra

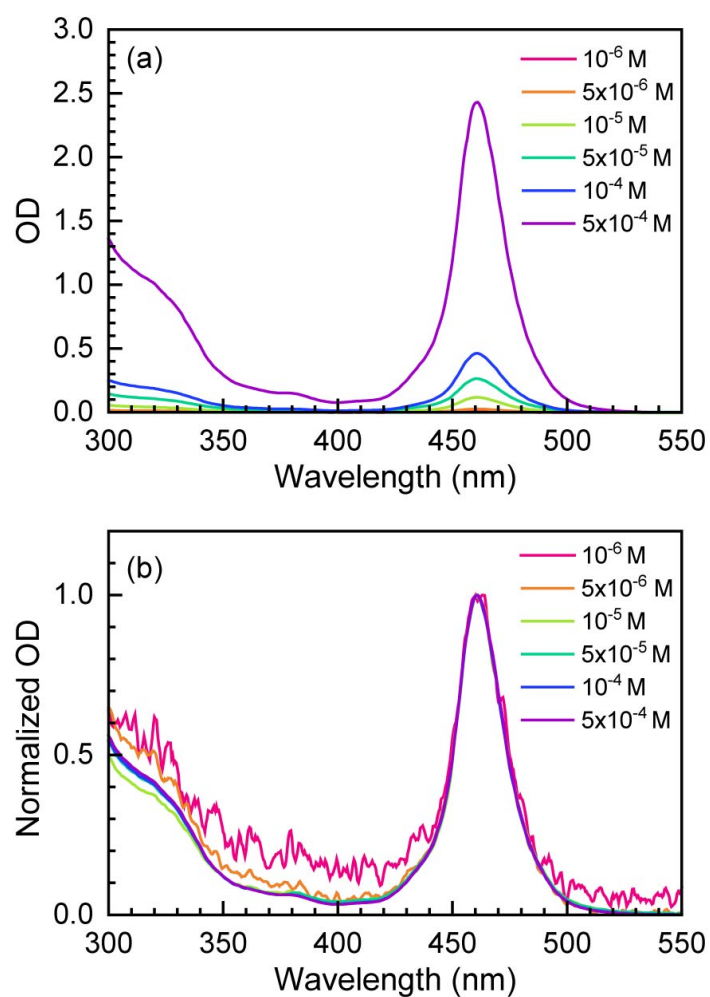


Fig. S5 Measured absorption spectra (a) and normalized spectra (b) of Np-2CzB at different concentrations in DCM solution.

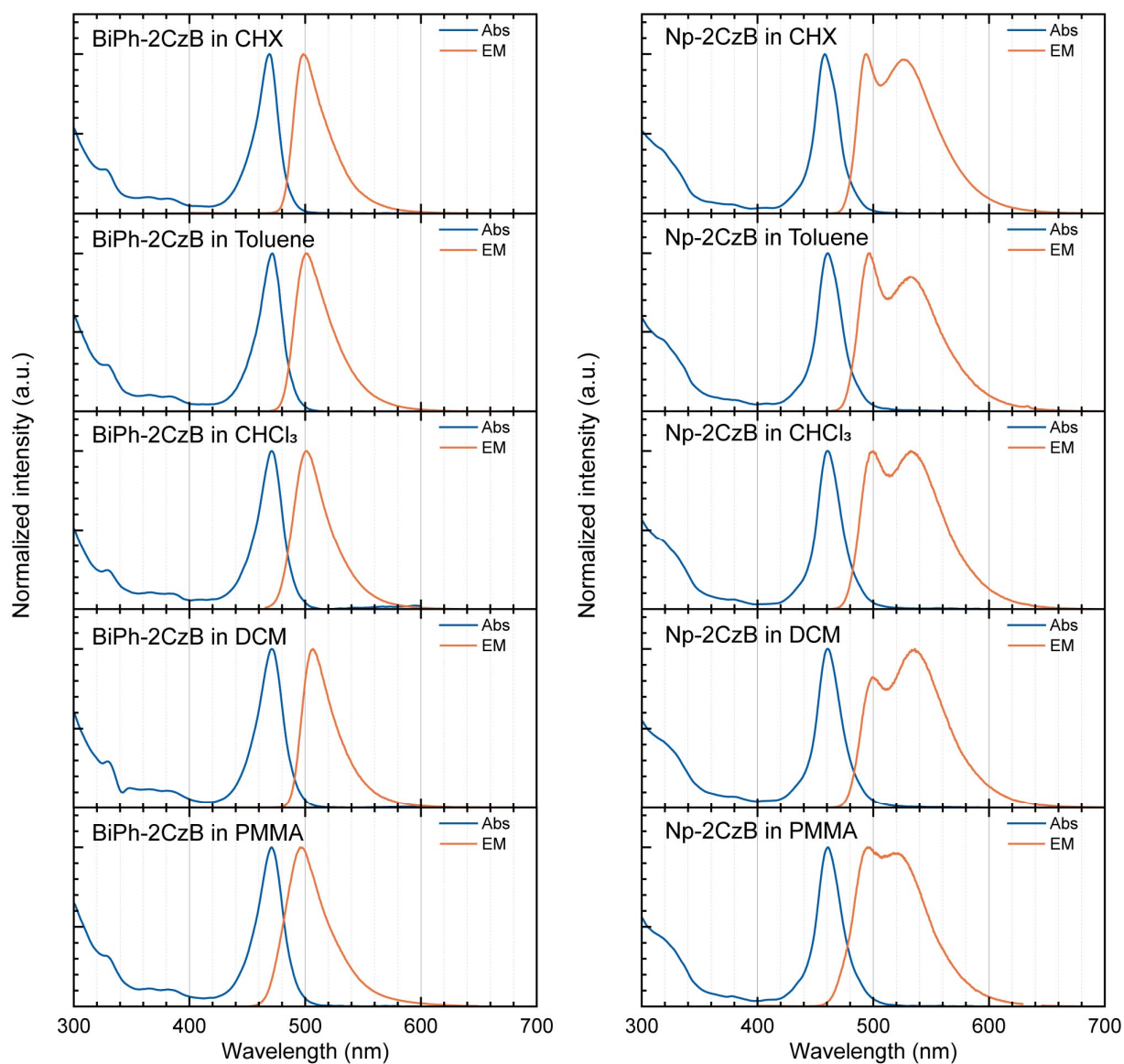


Fig. S6 Measured absorption (blue lines) and fluorescence (orange lines) spectra of BiPh-2CzB (left column) and Np-2CzB (right column) in different solvents and PMMA doping films.

Section S5. Time-resolved Fluorescence

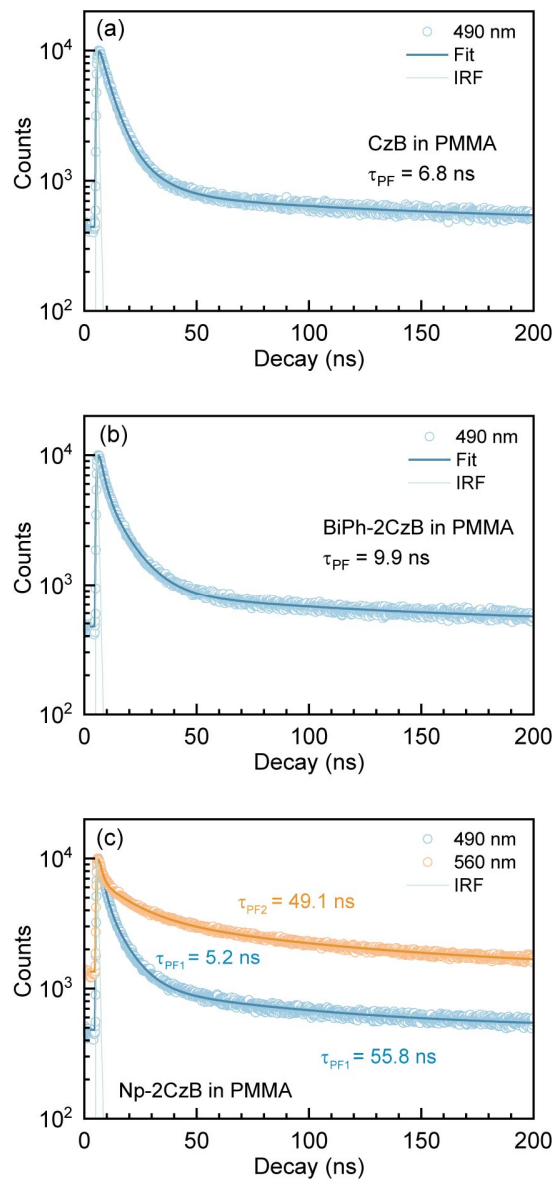


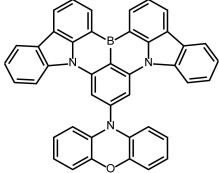
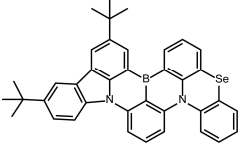
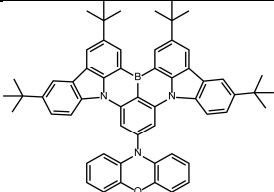
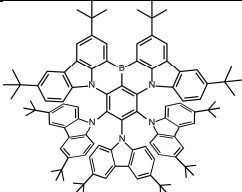
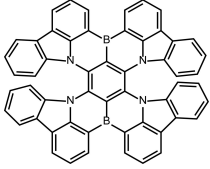
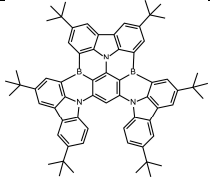
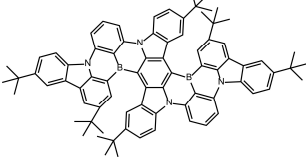
Fig. S7 The measured PF decay traces of CzB (a), BiPh-2CzB (b), Np-2CzB (c) in PMMA doping films upon optical excitation at 320 nm.

Section S6. Reported k_{RISC} values of reported TADF emitters

Table S2. Reported k_{RISC} values of several typical CT-type TADF emitters in dilute solutions.

| Name | Structure | k_{RISC} (10^5 s^{-1}) | Ref. |
|------------------------|-----------|------------------------------------------------|---------------------------------------------------------|
| 4CzIPN | | 8.8 | <i>Nat. Mater.</i> 2019 , 18 (10), 1084–1090. |
| PXZ-DPS | | 2.4 | <i>Nat. Photon.</i> 2014 , 8 (4), 326–332. |
| 5CzBN | | 2.2 | <i>Nat. Mater.</i> 2019 , 18 (10), 1084–1090. |
| AQ(PhDPA) ₂ | | 1.2 | <i>J. Phys. Chem. C</i> 2018 , 122, 3727–3737 |
| DMAC-DPS | | 0.9 | <i>Nat. Photon.</i> 2014 , 8 (4), 326–332. |
| PzTDBA | | 0.5 | <i>Chem. Sci.</i> 2024 , 15 (17), 6410–6420. |
| TPA-TOSBA | | 0.2 | <i>J. Phys. Chem. Lett.</i> 2022 , 13, 7561–7567 |
| CzDBA | | 0.05 | <i>Nat. Photon.</i> 2018 , 12 (4), 235–240. |

Table S3. Reported k_{RISC} values of several typical B,N-MR emitters in dilute solutions.

| Name | Structure | k_{RISC} (10^5 s^{-1}) | Ref. |
|---------|-------------------------------------------------------------------------------------|------------------------------------------------|-------------------------------------------------------------|
| CzBN1 |  | 20 | <i>J. Am. Chem. Soc.</i> 2023 , 145, 12550–12560. |
| BN-Se |  | 16.0 | <i>J. Am. Chem. Soc.</i> 2022 , 144, 22976–22984. |
| CzBN3 |  | 3.27 | <i>J. Am. Chem. Soc.</i> 2023 , 145, 12550–12560. |
| BBCz-G |  | 1.8 | <i>J. Am. Chem. Soc.</i> 2020 , 142, 19468–19472. |
| R-BN |  | 0.67 | <i>Angew. Chem. Int. Ed.</i> 2021 , 60, 20498–20503. |
| BBCz-DB |  | 0.19 | <i>J. Am. Chem. Soc.</i> 2020 , 142, 19468–19472. |
| BBCz-R |  | 0.12 | <i>J. Am. Chem. Soc.</i> 2020 , 142, 19468–19472. |

Section S7. Calculated and experimentally measured excitation energy

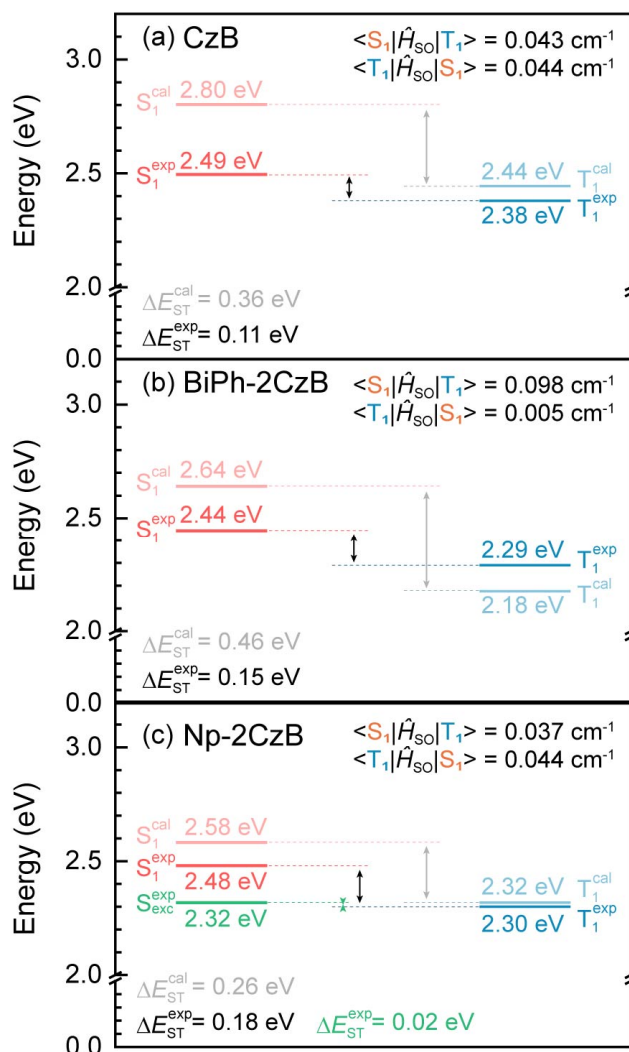


Fig. S8 The TDDFT calculated (B3LYP/6-31g*) adiabatic and experimentally measured energy of S_1 (red lines) and T_1 (blue lines) states of CzB (a), BiPh-2CzB (b) and Np-2CzB (c), as well as measured energy of excimer state (S_{exc} , green line) of Np-2CzB. The corresponding values of ΔE_{ST} and SOC matrix elements are provided as well.

Section S8. Reduced density gradient (RDG) analysis

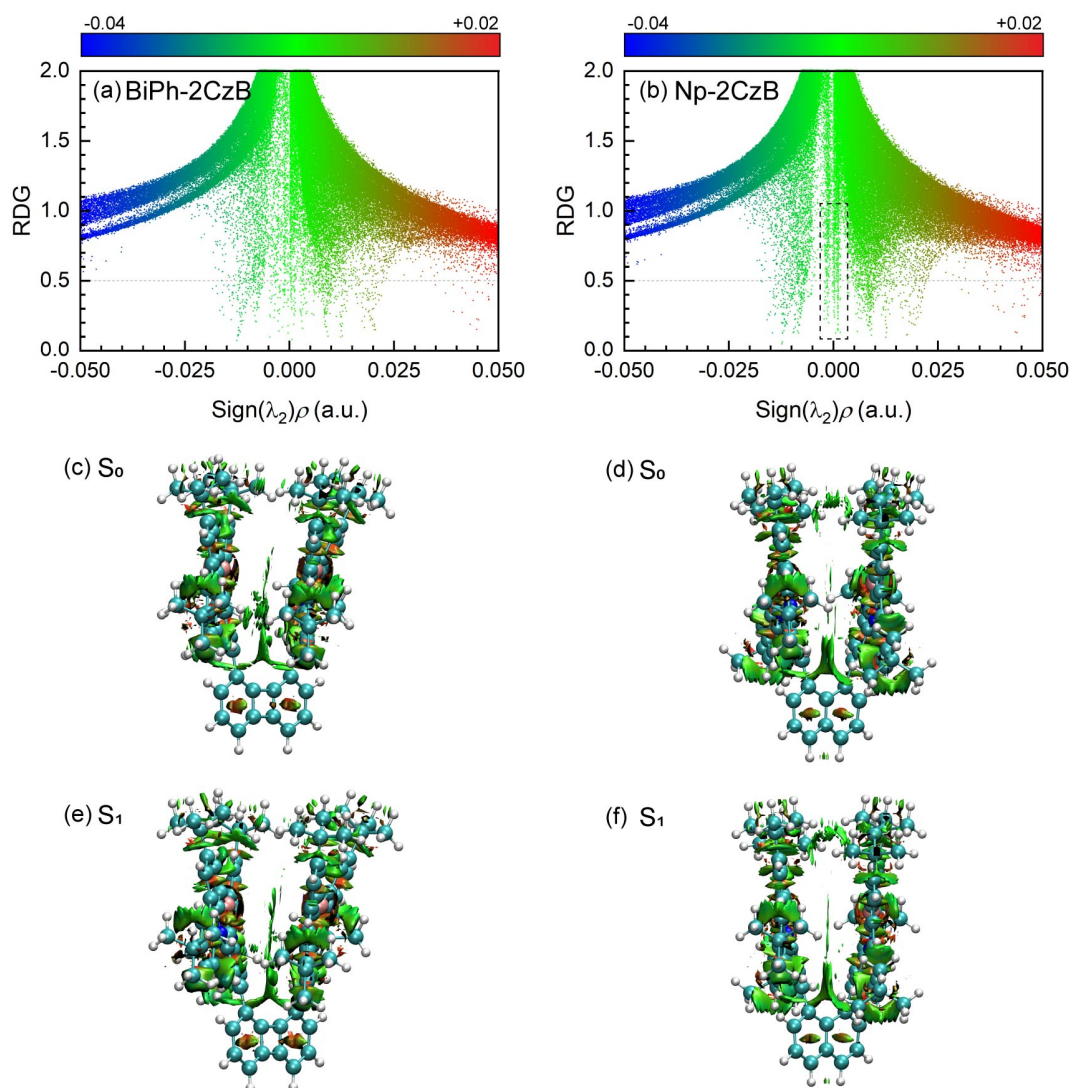


Fig. S9 Calculated reduced density gradient (RDG) scattering diagrams based on S_0 state geometry of BiPh-2CzB (a) and Np-2CzB (b), the corresponding RDG iso-surface of S_0 and S_1 state of BiPh-2CzB (c) (e) and Np-2CzB (d) (f) were also displayed.

Section S9. Vibrational analysis

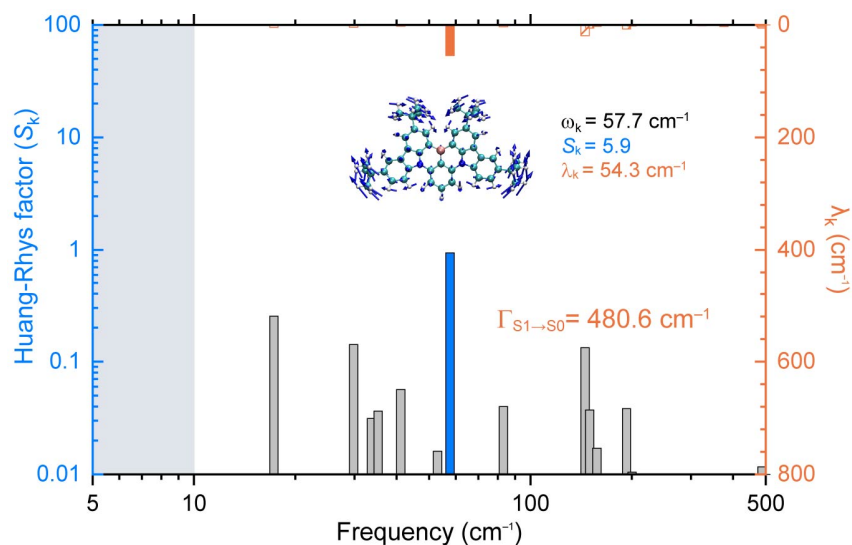


Fig. S10 Calculated Huang-Rhys factor (S_k) and reorganization energy contribution (λ_k) of each vibrational mode of CzB for the $S_1 \rightarrow S_0$ transition in toluene solution.

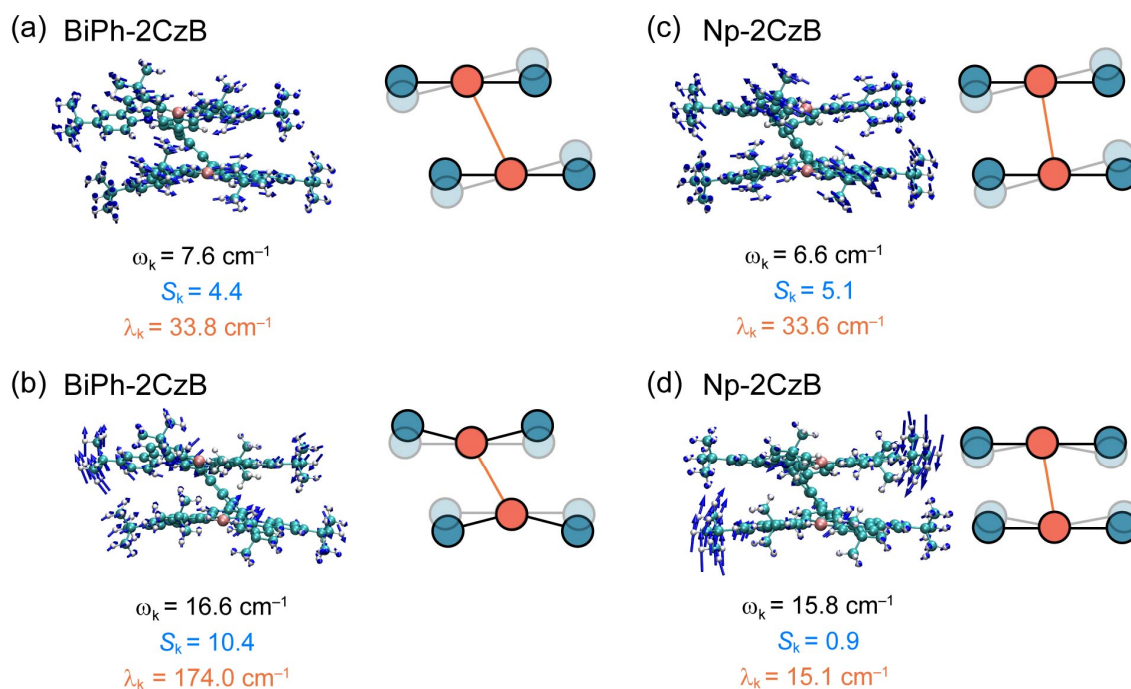


Fig. S11 Promoting vibrational modes of BiPh-2CzB (left) and Np-2CzB (right) for the $S_1 \rightarrow S_0$ transition, the Huang-Rhys factor (S_k) and reorganization energy contribution (λ_k) of these promoting modes are shown as well. Blue and red circles represent nitrogen and boron atoms in B,N-MR frameworks, respectively.

Section S10. Excitation-dependent fluorescence spectra

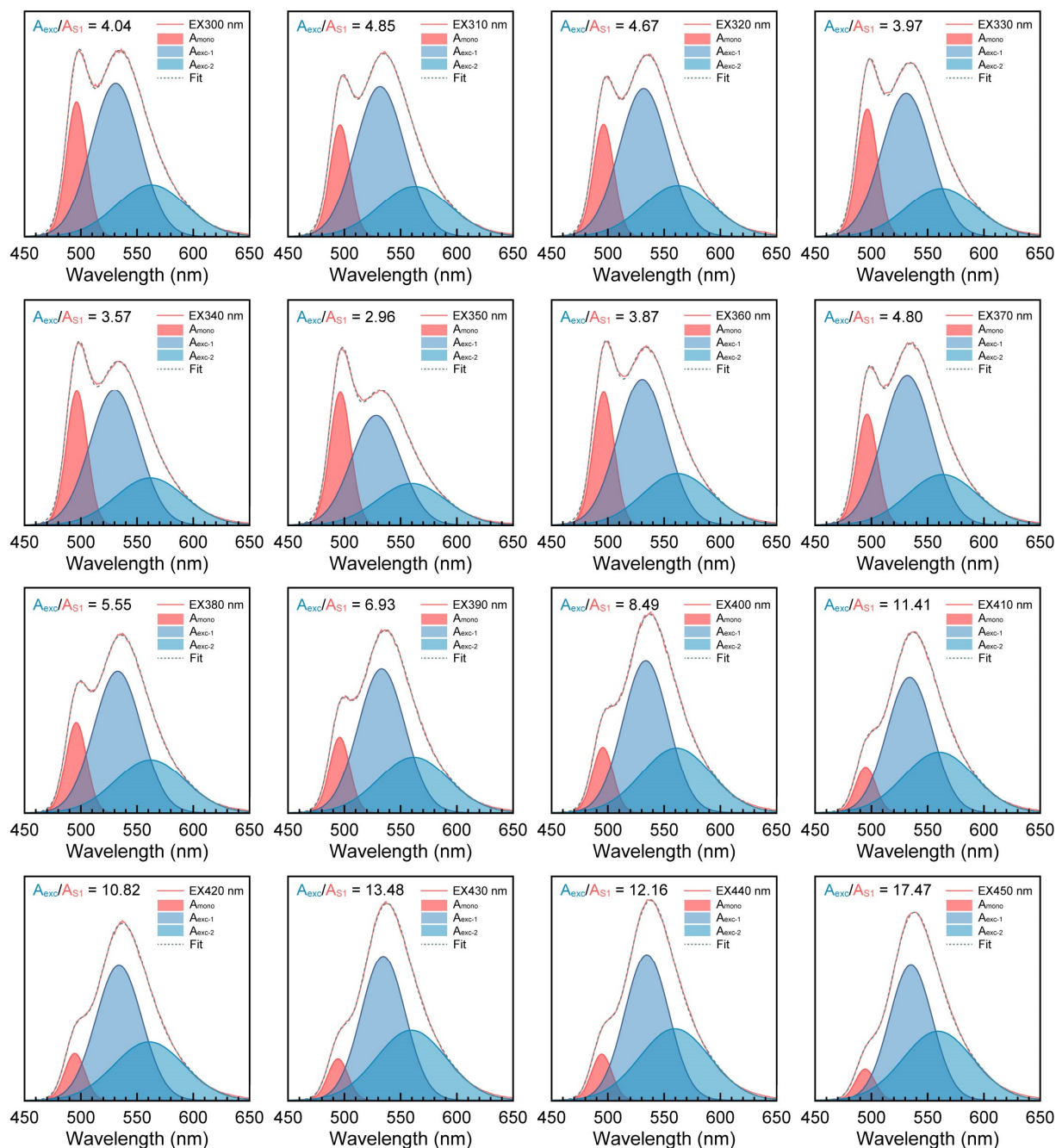


Fig. S12 The multi-Gaussian fitting excitation-dependent ($\lambda_{ex} = 300\text{--}450$ nm) emission spectra of Np-2CzB in DCM solution.

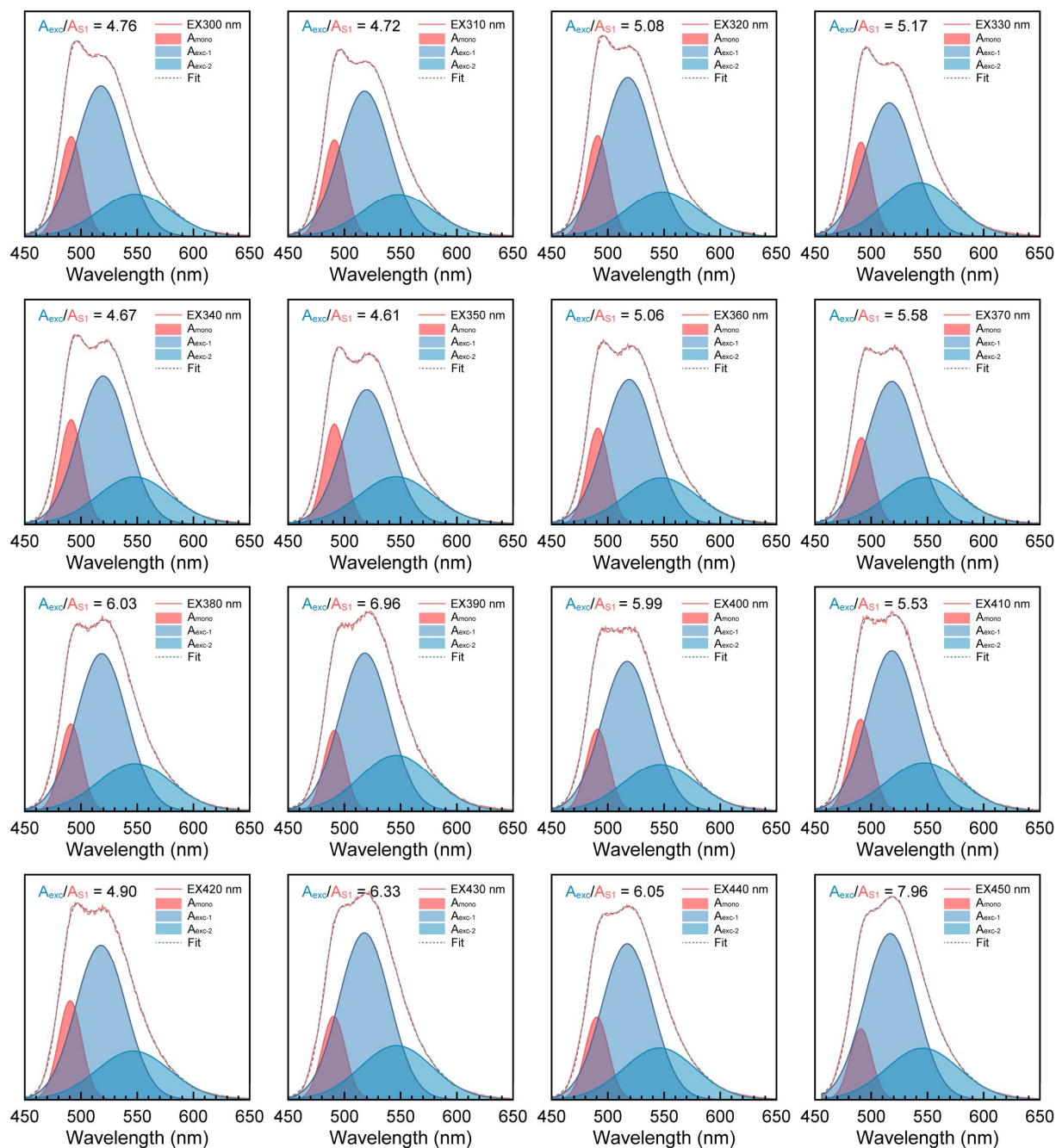


Fig. S13 The multi-Gaussian fitting excitation-dependent ($\lambda_{ex} = 300\text{--}450\text{ nm}$) emission spectra of Np-2CzB in PMMA doping films.

Section S11. fs-TA spectra

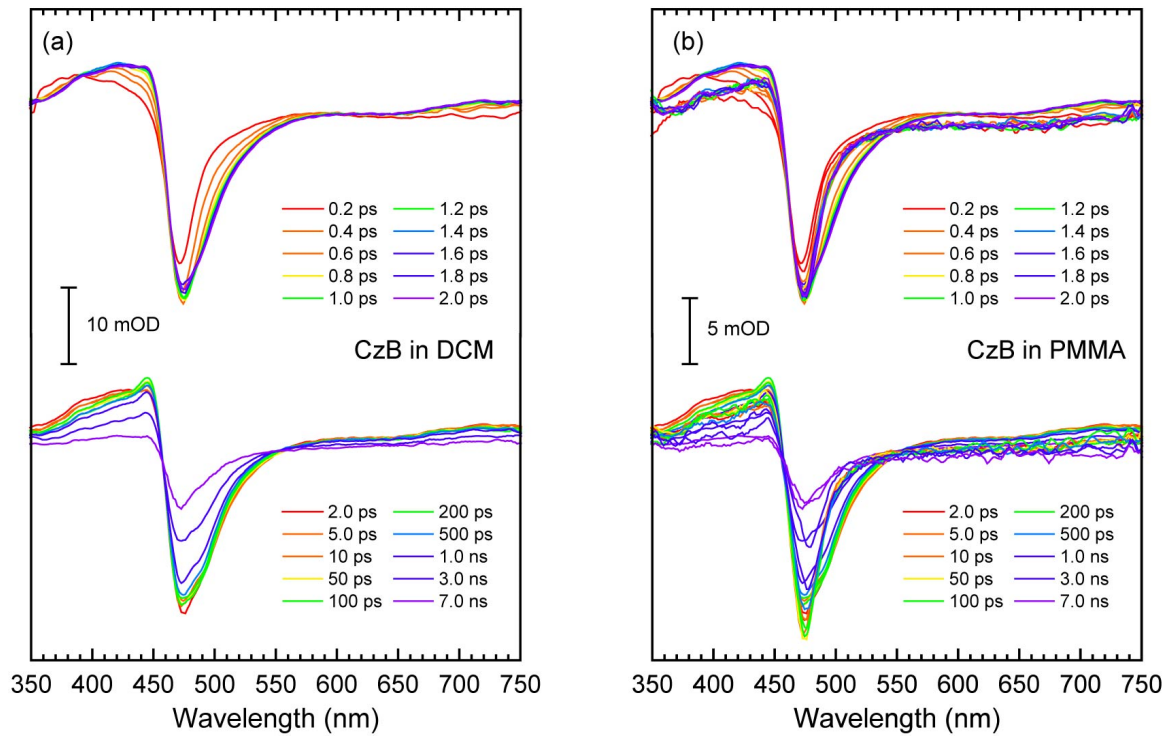


Fig. S14 Measured fs-TA spectra of CzB in DCM solution (a) and PMMA doping films (b) at selected delay times upon optical excitation at 320 nm.

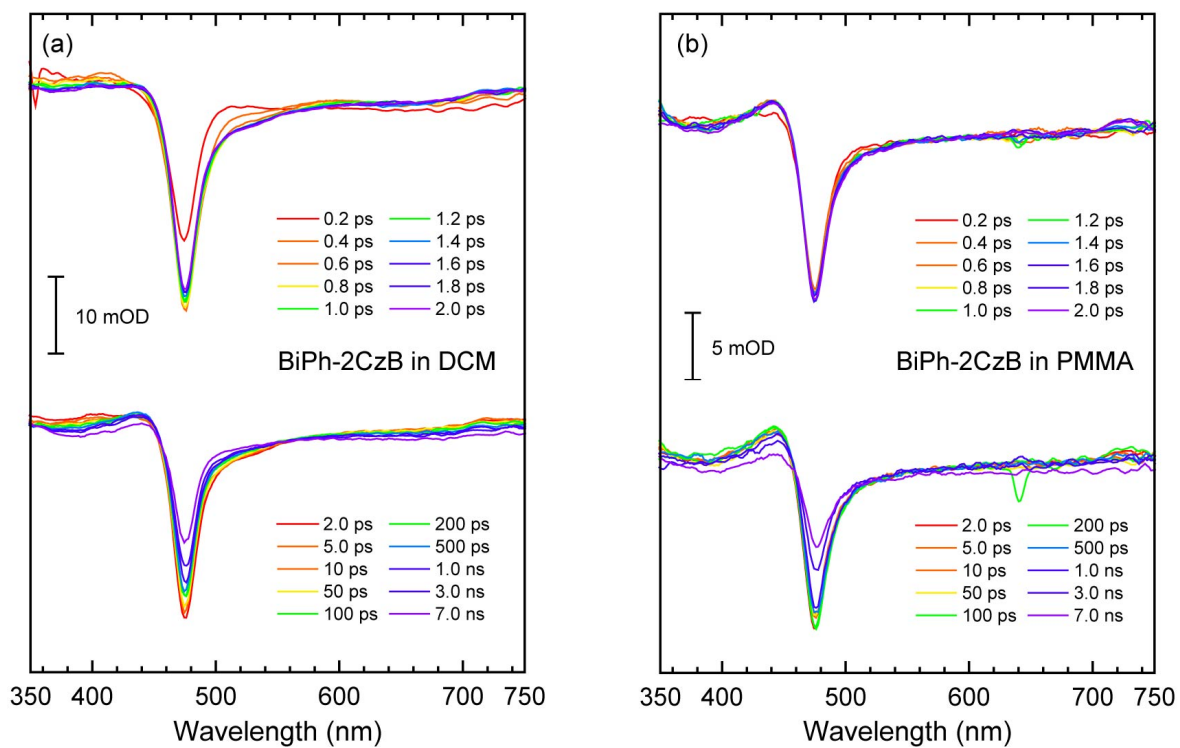


Fig. S15 Measured fs-TA spectra of BiPh-2CzB in DCM solution (a) and PMMA doping films (b) at selected delay times upon optical excitation at 320 nm.

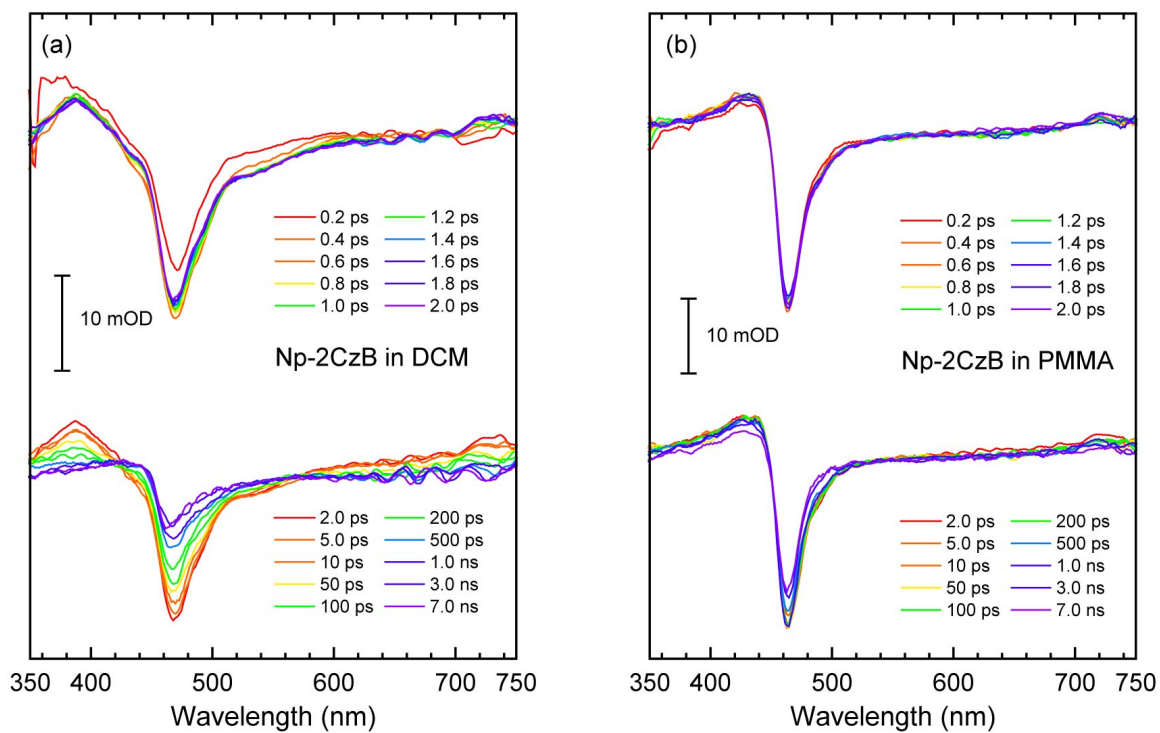


Fig. S16 Measured fs-TA spectra of Np-2CzB in DCM solution (a) and PMMA doping films (b) at selected delay times upon optical excitation at 320 nm.

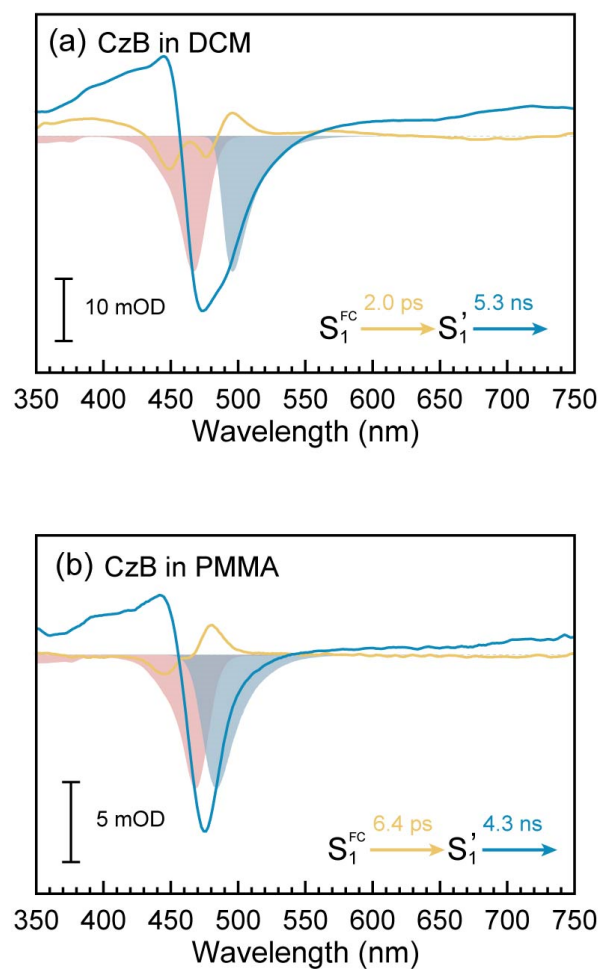


Fig. S17 The target analysis (sequential model) reconstructed extracted decay-associated spectra (DAS) from fs-TA spectra of CzB in DCM solution (a) and PMMA doping films (b) upon optical excitation at 320 nm.

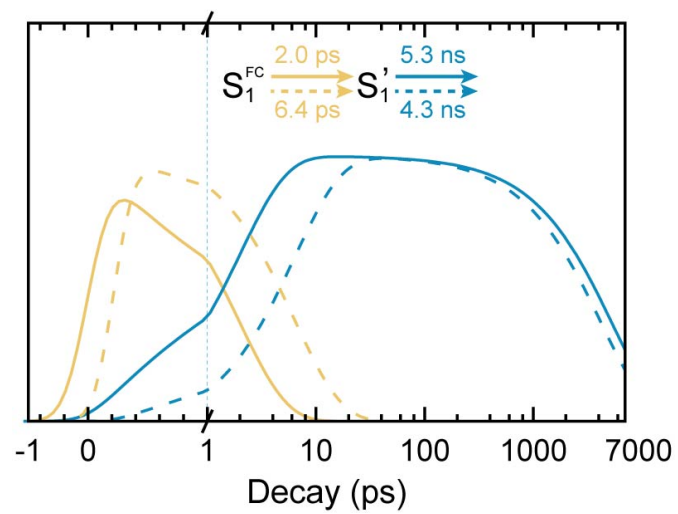


Fig. S18 Concentration evolution of transient species extracted from fs-TA of CzB in DCM solution (solid lines) and PMMA doping films (dash lines).